Estimates of net CO_2 flux by application of equilibrium boundary layer concepts to CO_2 and water vapor measurements from a tall tower

Brent R. Helliker,[1] Joseph A. Berry,[1] Alan K. Betts,[2] Peter S. Bakwin,[3] Kenneth J. Davis,[4] A. Scott Denning,[5] James R. Ehleringer,[6] John B. Miller,[3] Martha P. Butler,[4] and Daniel M. Ricciuto[4]

Received 12 January 2004; revised 2 July 2004; accepted 21 July 2004; published 19 October 2004.

[1] Convective turbulence within the atmospheric boundary layer (ABL) and movement of the ABL over the surface results in a large spatial (10^4–10^5 km^2) integration of surface fluxes that affects the CO_2 and water vapor mixing ratios. We apply quasi-equilibrium concepts for the terrestrial ABL to measurements of CO_2 and water vapor made within the ABL from a tall tower (396 m) in Wisconsin. We suppose that CO_2 and water vapor mixing ratios in the ABL approach an equilibrium on timescales longer than a day: a balance between the surface fluxes and the exchange with the free troposphere above. By using monthly averaged ABL-to-free-tropospheric water vapor differences and surface water vapor flux, realistic estimates of vertical velocity exchange with the free troposphere can be obtained. We then estimated the net surface flux of CO_2 on a monthly basis for the year of 2000, using ABL-to-free-tropospheric CO_2 differences, and our flux difference estimate of the vertical exchange. These ABL-scale estimates of net CO_2 flux gave close agreement with eddy covariance measurements. Considering the large surface area which affects scalars in the ABL over synoptic timescales, the flux difference approach presented here could potentially provide regional-scale estimates of net CO_2 flux. *INDEX TERMS:* 1615 Global Change: Biogeochemical processes (4805); 1818 Hydrology: Evapotranspiration; 3307 Meteorology and Atmospheric Dynamics: Boundary layer processes; 3322 Meteorology and Atmospheric Dynamics: Land/atmosphere interactions; *KEYWORDS:* boundary layer, CO_2 exchange, evapotranspiration

Citation: Helliker, B. R., J. A. Berry, A. K. Betts, P. S. Bakwin, K. J. Davis, A. S. Denning, J. R. Ehleringer, J. B. Miller, M. P. Butler, and D. M. Ricciuto (2004), Estimates of net CO_2 flux by application of equilibrium boundary layer concepts to CO_2 and water vapor measurements from a tall tower, *J. Geophys. Res.*, *109*, D20106, doi:10.1029/2004JD004532.

1. Introduction

[2] A worldwide, integrated system of measurements and models is under development for interpreting and predicting the role of terrestrial ecosystems in the global carbon balance [*Tans et al.*, 1990; *Denning et al.*, 1995; *Ciais et al.*, 1995; *Fung et al.*, 1997; *Ciais et al.*, 1997; *Baldocchi et al.*, 2001; *Keeling et al.*, 1989; *Conway et al.*, 1994]. Currently, there are more than 150 sites worldwide where carbon balance is assessed continuously using eddy covariance and other methods. The average footprint, or area of surface flux integration, typically does not exceed 1 km^2. The next larger scale at which adequate closure occurs is at the global scale ($\sim 51 \times 10^7$ km^2), where data from the global flask network enables precise trace gas and isotope balance studies of the world's atmosphere [*Keeling et al.*, 1989; *Conway et al.*, 1994]. The scale intermediate to these extremes, the regional scale (broadly defined as 10^4 to 10^6 km^2), is relevant for studies of the effects of climate change and evaluating management decisions on the carbon cycle. Landscape heterogeneity and complex terrain complicates extrapolation from eddy covariance measurements to the regional scale, and sparse coverage by the global networks limits down scaling from the global to the regional scale [*Gurney et al.*, 2002]. Hence it is of considerable interest to develop measurement-based methodologies that can estimate net surface flux at the regional scale.

[3] The current analysis focuses on the atmospheric boundary layer (ABL) which the terrestrial surface locally modifies through evapotranspiration and physiological pro-

[1]Department of Global Ecology, Carnegie Institution of Washington, Stanford, California, USA.
[2]Atmospheric Research, Pittsford, Vermont, USA.
[3]Climate Monitoring and Diagnostics Laboratory, National Oceanic and Atmospheric Administration, Boulder, Colorado, USA.
[4]Department of Meteorology, Pennsylvania State University, University Park, Pennsylvania, USA.
[5]Department of Atmospheric Science, Colorado State University, Fort Collins, Colorado, USA.
[6]Department of Biology, University of Utah, Salt Lake City, Utah, USA.

0148-0227/04/2004JD004532$09.00

cesses such as photosynthesis and respiration, leading to changes in the mixing ratios of water vapor and CO_2. Meteorological processes such as the entrainment of tropospheric air during boundary layer growth, synoptic-scale subsidence of the troposphere, radiative processes, mesoscale circulations (e.g., sea breezes) and boundary layer cloud formation tend to counter the influence of the land surface by facilitating mixing between the ABL and the typically drier and warmer (potential temperature) overlying troposphere. For our purposes here, we use the traditional definition of the fair weather ABL of *Stull* [1988] to include the daytime convective, nocturnal stable and residual boundary layers. The ABL air mass is also moving over the land surface ($\sim$500 km d^{-1} under typical fair weather conditions, and dispersing in the horizontal due to divergence and wind shear [*Raupach et al.*, 1992]. Hence the composition of the ABL at any point above the land surface is a function of the initial composition of the air mass when the boundary layer was formed, exchanges with the surfaces over which it has passed, and the exchanges with tropospheric air that has mixed with it along its way.

[4] Studies of the CO_2 balance of the ABL have the potential to provide information on carbon balance of the land surface on a regional scale. Indeed, the surface area of integration by the ABL for one day was estimated to be 10^4 km^2 [*Raupach et al.*, 1992] and the surface footprint for the concentration of a trace gas of surface origin in the ABL has been estimated to be about 10^6 km^2 [*Gloor et al.*, 2001]. Many papers have described the scalar rate of change in the ABL during the nonlinear growth of the ABL over a diurnal (daytime) period [*De Bruin*, 1983; *McNaughton and Spriggs*, 1986; *Denmead et al.*, 1996; *Raupach*, 1995, 2000, 2001; *Levy et al.*, 1999; *Kuck et al.*, 2000; *Lloyd et al.*, 2001; *Styles et al.*, 2002], and the stable nocturnal accumulation [*Pattey et al.*, 2002]. These studies have demonstrated that budget methods for the period of daytime boundary layer growth can be used to estimate daytime surface fluxes. However, it is difficult to close these boundary layer budgets over complete diurnal cycles [cf. *Fitzjarrald*, 2002] making this approach impractical for long-term CO_2 balance estimates.

[5] In this paper we explore longer timescale averages using continuous observations of mixing ratio and flux of CO_2 and H_2O from a tall tower in north-central Wisconsin for one year (January to December 2000). The measurement height of 396 m is well within the convective boundary layer during the day and typically within the residual layer and above the stable nocturnal boundary layer at night [*Yi et al.*, 2001]. As illustrated in the work of *Yi et al.* [2001], the CO_2 mixing ratio measured at 396 m typically varies little over a composite diurnal cycle. Thus long-term averages of CO_2 measured continuously at 396 m represent an integration over successive diurnal cycles of modifications of ABL scalars by exchanges with the surface and the free troposphere. The fundamental shift of perspective from a focus on the growth of the daytime ABL to the slow evolution of the ABL, averaged over the diurnal cycle, and for much of the time nearly in balance with larger-scale subsiding circulations in based on the arguments of *Betts* [2000, 2004] and *Betts et al.* [2004]. *Betts* [2000] suggests that the complex diurnal dynamics of the ABL over land are on longer timescales captive to large-scale atmospheric processes. The ABL is an integral component in large-scale circulation as it connects the ascending and descending branches of the atmospheric circulation. Water vapor evaporated from the surface is carried aloft by convection in the ascending branches and condenses as it ascends. The resultant latent heat release warms the upper atmospheric air, which descends as it radiatively cools in the subsiding branches. On a global average, vertical transport by convective storm processes results in complete replacement of ABL air every four days [*Cotton et al.*, 1995]. *Betts and Ridgway* [1989] developed an equilibrium model for the ABL under the subsiding branch over the tropical oceans, showing that radiatively driven subsidence, radiative cooling and the surface fluxes were in balance. *Betts* [2000] recognized that a similar surface ABL equilibrium exists over land and applied an equilibrium approach by averaging the ABL over the diurnal cycle. The underlying assumption is that the ABL approaches a steady state or equilibrium between the surface fluxes, cloud effects on radiation and subsidence of the overlying free troposphere over temporal scales larger than a day. The nonlinear processes of daytime ABL growth and the decoupling of the stable boundary layer at night are superimposed on this slowly evolving mean state. We know from the early decades of climate modeling, when the diurnal cycle was routinely ignored to reduce computational costs, that the mean ABL climate can be modeled with fair realism in this way, but with what approximation remains unclear. *Betts* [2000] demonstrated that the idealized equilibrium model approach was a reasonable fit to composites of modeled European Centre (ECMWF) and observed (Kansas grassland experiment data from *Betts and Ball* [1998]) ABL potential temperature and water vapor. More recently, *Betts* [2004] showed that the 24-hour mean state and fluxes describe well the climate transitions and coupling over land using 30 years of the fully time-dependent, ECMWF reanalysis model data. *Betts et al.* [2004] extended this idealized model to show how the mixed layer equilibrium of water vapor, CO_2, and radon was coupled to the respective surface fluxes via mass exchange with the free troposphere during periods of large-scale subsidence.

[6] On monthly timescales, continuous measurements of CO_2 in the ABL from tall towers show distinct differences from the background CO_2 in the Marine Boundary Layer (MBL) [*Bakwin et al.*, 1998]. Here we suggest that these distinct differences of CO_2 reflect a near-equilibrium or steady state balance between surface uptake/release and free-tropospheric exchange. Assuming the near balance between surface evapotranspiration and the flux of dry, free-tropospheric air into the ABL, on timescales longer than a day, we can make an observational estimate of the mass exchange with the free troposphere in undisturbed conditions. By assuming similar transports for water vapor and CO_2, we shall estimate the surface net ecosystem exchange (NEE) from the concentration differences of CO_2 between the free troposphere (FT) and the ABL, and compare this with surface NEE measurements. The vertical velocity implied by the exchange fluxes between the ABL and FT should be similar to estimates for subsidence of the troposphere. Precipitation and evaporation processes violate the assumption of similar transport for CO_2 and water vapor, so we assess the impact of this by filtering our data

to exclude days with precipitation and by the amount of precipitation. Initially, we tested these ideas using a summer period [*Helliker et al.*, 2002], which we have extended here to a full year of data. Subsequently, *Bakwin et al.* [2004] adopted a similar approach to calculate net surface CO_2 flux from average CO_2 concentrations at four towers (including this tower) using solely vertical velocity estimated from model data (the NCEP reanalysis).

[7] The boundary layer budget equation [e.g., *Betts*, 1992; *Raupach et al.*, 1992; *Denmead et al.*, 1996; *Levy et al.*, 1999; *Kuck et al.*, 2000; *Lloyd et al.*, 2001] for CO_2 can be written (see Appendix A, equation (A2)) neglecting horizontal advection as

$$\rho h \frac{\partial C_m}{\partial t} = F_{NEE} - \rho W(C_t - C_m), \quad (1)$$

which describes the storage change in the ABL of depth h in terms of the difference of a surface flux and a flux exchange with the free troposphere. W is the effective mixing velocity between ABL and free-tropospheric air (m s^{-1}) and ρ is density of air at the height of W. F_{NEE} is the net ecosystem exchange (NEE; μmol m^{-2} s^{-1}, but also given as F_{NEE}/ρ in units of ppmv m s^{-1}) of CO_2 flux averaged over some time interval. C_m, C_t are mean mixing ratios of CO_2 in the ABL and free troposphere, respectively. As the averaging period increases, the storage term becomes small compared to the flux terms (see Appendix A) allowing us to write the following pair of equations, which are analogous to equations (31) and (33) in the work of *Betts et al.* [2004]:

$$F_{NEE} = \rho W(C_t - C_m). \quad (2)$$

A similar equation can be written for water vapor mixing ratio (q) and net flux (F_q; mmol m^{-2} s^{-1})

$$F_q = \rho W(q_t - q_m). \quad (3)$$

Significantly, the net surface flux of evaporation is much easier to measure and model than CO_2. If F_q, q_m and q_t are known, and assuming that ρW is the same for all scalars, then by rearranging (3), an estimate can be made of ρW, which will hereafter be referred to as the ABL flux difference estimate, ρW_{FD}

$$\rho W_{FD} = \frac{F_q}{(q_t - q_m)}. \quad (4)$$

We will then substitute equation (4) in equation (2) to give an estimate of F_{NEE} from $C_t - C_m$, which will be compared with eddy correlation measurements from the WLEF tower, located in a fairly homogeneous, forested region in north-central Wisconsin. This is an observationally based estimate of the mass exchange of the ABL with the free troposphere. From this platform, mixing ratios C_m and q_m are measured at a height of 396 m, and these values can be taken as direct estimates of means for the ABL. However, we must make two primary assumptions for ABL-scale water vapor flux and the free-tropospheric boundary conditions: (1) F_q measured by eddy covariance methods at 122 m from the tower is representative of the same surface scale which affects C_m and q_m and (2) on a monthly timescale, free-tropospheric mixing ratios above the tower can be represented by proxy measurements. C_t was obtained from the marine boundary layer at the same latitude of the WLEF tower and q_t from hourly analyses from a weather forecast model (Globalview-CO_2 2003, Rapid Update Cycle; see http://maps.fsl.noaa.gov/ and ftp.cmdl.noaa.gov,Path:ccg/co2/GLOBALVIEW). Estimates of ρW were also obtained from NCEP/NCAR reanalysis-2 model data (NOAA-CIRES Climate Diagnostics Center, Boulder, Colorado, USA at http://www.cdc.noaa.gov/) for comparison with ρW_{FD} to assess whether this vertical mass exchange derived from the steady state assumption is consistent with the large-scale subsidence.

2. Methods of Analysis

2.1. Study Site

[8] This study was performed in NW Wisconsin, USA, on and around the WLEF television broadcast tower (45.9°N, 90.3°W) as part of the Chequamegon Ecosystem-Atmosphere Study (http://cheas.psu.edu/). The tower is 450 m tall and located within the Chequamegon-Nicolet National Forest and is a NOAA-CMDL CO_2 sampling site [*Bakwin et al.*, 1998]. The area is largely forested for hundreds of km to the east and west, Lake Superior is approximately 70 km to the north and agriculture begins to dominate about 200 km to the south. The dominant forest types are mixed northern hardwood, aspen, and wetlands. The population density for the area is approximately five people per square km.

2.2. Continuous Measurements of ABL CO_2 and H_2O

[9] Measurements of ABL CO_2 (C_m) and H_2O (q_m) mixing ratios were obtained at 396 m on the WLEF tower [*Bakwin et al.*, 1998]. Measurements of surface water vapor flux (F_q) were obtained from eddy covariance (EC) measurements at 122 m from the tower [*Davis et al.*, 2003]. Note that the flux data were not gap filled and hence comparisons of F_{NEE} and NEE at 122 m from the WLEF tower were made only when measurements of F_q from 122 m were available. The EC flux data do, however, include corrections for daily changes in scalar storage.

2.3. Measurements of CO_2 and H_2O in the Free Troposphere

[10] On 19, 23 and 24 August 2000, CO_2 and H_2O mixing ratios were obtained directly from airplane flights from 5 km above the WLEF study site. Similar measurements were made for six additional days spanning the month of August for the midwestern United States as part of the CO_2 budget and rectification airborne study (COBRA; *Gerbig et al.* [2003]; http://www-as.harvard.edu/chemistry/cobra/index.html). The mean of these values was used for free tropospheric values over the WLEF site for the month of August.

[11] The free troposphere values of CO_2 (C_t) and H_2O (q_t) over WLEF were extended to the full year with proxies to supplement the sparse data from aircraft flights. C_t, as measured by airplane flights above 4 km in August 2000, was fairly constant over the entire midwest (366.7 ± 1.8 ppmv), and the mean value of CO_2 was about two

Table 1. Percentage of Days in a Month That Were Averaged to Obtain Monthly Averages of C_m, q_m, F_q, and NEE_{EC} Based on Average Precipitation Data for a Given Day

	Percent of Days in Flux Difference Analysis			
Month	ppt < 1 mm	ppt < 2 mm	ppt < 5 mm	All Days
Jan.	93.5	100.0	100.0	100.0
Feb.	79.3	93.1	93.1	100.0
Mar.	74.2	87.1	93.5	100.0
Apr.	70.0	73.3	86.7	100.0
May	77.4	83.9	87.1	100.0
June	56.7	60.0	80.0	100.0
July	71.0	80.6	90.3	100.0
Aug.	74.2	80.6	93.5	100.0
Sept.	76.7	83.3	93.3	100.0
Oct.	83.9	90.3	96.8	100.0
Nov.	70.0	80.0	90	100.0
Dec.	100.0	100	100	100.0
Annual	77.3	84.4	92.1	100.0
May–Sep.	71.2	77.8	88.9	100.0

ppmv different from the monthly mean of CO_2 from the marine boundary layer (MBL) (GLOBALVIEW-CO_2 2003; see ftp.cmdl.noaa.gov,Path:ccg/co2/GLOBALVIEW) at a similar latitude to the WLEF tower (44.4°). The continuous (and flask) measurements at the towers and the flask measurements at all other sites, which are used to calculate the MBL surface product, are all directly traceable to the WMO CO_2 mole fraction scale, maintained by NOAA/CMDL. On the basis of comparisons of the simultaneous continuous and flask records at the NOAA/CMDL observatories (Barrow, Mauna Loa, Samoa, and South Pole), flask and continuous measurements agree to within 0.1 ppm [*King and Schnell*, 2002]. We chose to use the MBL as a reference system for analysis of net CO_2 flux at WLEF. According to the equilibrium boundary layer concept, the mean value of C_m should be approximately equal to the corresponding mean C_t if net CO_2 flux over the ocean surface is negligible. Given the strong zonal flow of the upper atmosphere at these latitudes, C_t over the mid continent should be similar to that over the oceans.

[12] Aircraft measurements of average q_t in the upper midwest United States for the month of August (2.3 ± 1.2 g/kg) were similar to q_t derived from Rapid Update Cycle (RUC; 1.8 ± 0.08 g/kg; http://maps.fsl.noaa.gov/) weather forecasting data from geopotential heights of 3000 to 3700 m (above sea level, the ground elevation at WLEF is about 500 m above sea level). RUC is a high frequency weather prediction system developed as a service to provide short-range weather forecasts. The model is updated every 3 hours with observations from (but not limited to) surface weather stations, commercial aircraft, various sondes and satellite-derived data for the contiguous United States. Direct measurements of q_t available for August agreed well with the RUC estimates on a monthly averaged basis. A full test of RUC versus observed q_t for a continuous time series would be ideal, but this was not possible. To partially compensate, we tested the continuous time series of observed ABL q_m from the WLEF tower versus RUC outputs at a similar height. q_m available from the WLEF tower (measured at 396 m) for June through September of 2000 were highly correlated ($y = 0.94x + 0.2462$, $r^2 = 0.92$) with q obtained from RUC data (geopotential heights of 300–600 m). A similarly good agreement was not found with other model sources of q_m such as the NCEP/NCAR Reanalysis-2 data ($y = 1.11x - 0.1592$ $r^2 = 0.29$). We used direct measurements of C_m and q_m from the tower and proxies (the CO_2 from the MBL for C_t, and the RUC data for q_t,) to construct the mean differences in CO_2 and water vapor concentration for the full year of 2000.

2.4. Estimating ρW From Reanalysis Data

[13] For comparison with ρW_{FD} derived from (4), we estimated ρW at 700 mb from the 24h "daily average" pressure vertical velocity (Ω; Pa s^{-1}) of the NCEP/NCAR Reanalysis-2 data (provided by the NOAA-CIRES Climate Diagnostics Center, Boulder, Colorado, USA at http://www.cdc.noaa.gov/), using

$$W\rho_{\Omega} = -\Omega/g, \tag{5}$$

where g is gravitational acceleration.

2.5. Data Averaging, Selection, and Filtering

[14] C_m, q_m measured continuously at 396 m and F_q, net ecosystem exchange measured by eddy covariance (NEE_{EC}) measured at 122 m were averaged over 24h periods for the year 2000. If any day was missing more than 3 hours of data for any of the above variables, that day was excluded from the analysis, reanalysis-2 data were also excluded on these days. This resulted in a loss of about 14% of days annually. Twenty-four hour sums of precipitation measured at the WLEF tower (pptT) and at a separate site 15 km to the southeast (pptT_15km) were used to select for subsidence-dominated, or "fair weather" days by eliminating days with precipitation greater than a given threshold, where

$$\text{ppt} = (\text{pptT} + \text{pptT\_15 km})2. \tag{6}$$

We then formed monthly averages by selecting those days with ppt less than a threshold. For example, for ppt < 1 mm, which we consider representative of fair weather days, the monthly averages include all days receiving less than 1 mm precipitation per day. We then derived averages with higher thresholds; ppt < 2 mm, ppt < 5 mm and the final monthly average consisted of all of the available days for analysis, and will be referred to as "all days." Table 1 presents the percentage of daily data that was used to calculate ρW_{FD}, and F_{NEE}, for each precipitation threshold. To illustrate our method of calculations: for ppt < 1 mm, ρW_{FD} was determined by (3) for a given month by averaging the 24 hour values of F_q, q_m and q_t for days when ppt < 1 mm. F_{NEE} was calculated over this period by (1) and the average of 24 hour values of C_m and C_t when ppt < 1 mm. These values of F_{NEE} were compared to the NEE_{EC} values averaged for days with the same ppt threshold.

3. Results and Discussion

3.1. Long-Term CO_2, Free-Tropospheric Boundary Conditions, and Equation Variables

[15] 24 hour averages of CO_2 measured continuously at 396 m (C_m) for the month of August are presented in Figure 1a, along with the monthly average of free-tropospheric CO_2 and surface pressure. C_t in Figure 1a is an average (± standard error) of the CO_2 measured directly

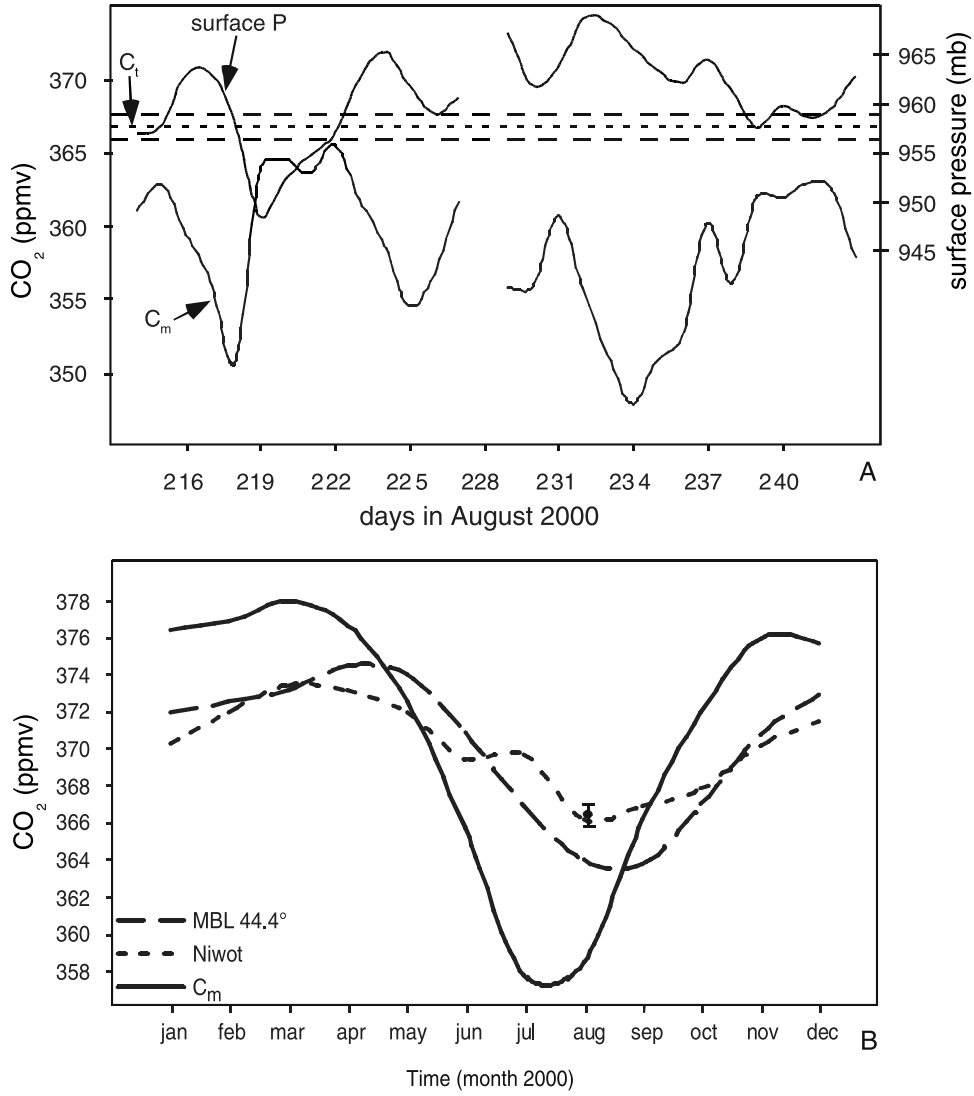

Figure 1. (a) Twenty-four hour averages of CO_2 measured continuously at 396 m (C_m), direct measurements of free-tropospheric CO_2 (C_t), and surface pressure for the month of August 2000. C_t is an average (large dashed lines equal standard error) of the CO_2 measured directly by the COBRA campaign over the entire midwestern United States for the month of August. (b) Monthly averages of CO_2 in the marine boundary layer (MBL) at 44.4°N (long-dashed line), from 3475 m from atop Niwot Ridge, CO, 40.1°N (short-dashed line), and from 396 m from the WLEF tower, 45.9°N (C_m). The single point and error bars represent the monthly mean and standard error for CO_2 measured above 4500 m by the COBRA airplane program over the midwestern United States in August of 2000. See color version of this figure in the HTML.

by the COBRA campaign over the entire midwestern United States for the month of August. C_m remains below C_t for nearly all 24 hour periods. When low-pressure systems move through the area, C_m approaches C_t due to the rapid vertical mixing associated with storms. Under persistent high-pressure periods when deep convection is suppressed, the net effects of predominant surface CO_2 uptake can be seen as a continual drawdown of C_m from day to day (i.e., days 214–218, 222–225, 230–234). This pattern would not be expected if the 396 m height sampled free tropospheric air at night, or if the stable nocturnal boundary layer grew to this height, both processes would increase the 24 hour average of CO_2. Thus we assume that, on average, CO_2 measured at 396 m was a continuous measure of the residual boundary layer at night and the convective boundary layer during the day. The mean 24 hour state of CO_2 appears to be a qualitative integration of the processes of respiration, photosynthesis and mixing of free tropospheric air which, over longer timescales, are slave to larger synoptic-scale processes. On timescales longer than 24 hours, undisturbed weather conditions are temporally dominant and averages of C_m qualitatively reflect the seasonal change in the predominant surface exchange of CO_2, with photosynthesis predominant in summer and respiration predominant in fall, winter and spring (Figure 1b).

[16] Figure 1b shows monthly ABL CO_2, two free-tropospheric proxies for CO_2 and the monthly mean of CO_2 measured directly by airplane flights (from the

Table 2. Monthly Means and Standard Error of ABL and Free-Tropospheric Mixing Ratios and Flux Estimates for CO_2 and Water Vapor for All Days[a]

Month	C_t, ppmv	C_m, ppmv	q_t, g/kg	q_m, g/kg	NEE_{EC}, μmol m^{-2} s^{-1}	F_q, μmol m^{-2} s^{-1}	$F_{NEE}(\rho W_{FD})$,[b] μmol m^{-2} s^{-1}
Jan.	371.9 ± 0.2	376.4 ± 0.5	0.8 ± 0.02	1.7 ± 0.2	0.2 ± 0.04	0.1 ± 0.03	0.6 ± 0.13
Feb.	372.4 ± 0.2	376.8 ± 0.4	0.9 ± 0.03	2.8 ± 0.3	0.3 ± 0.04	0.1 ± 0.03	0.3 ± 0.06
Mar.	373.1 ± 0.2	377.9 ± 0.6	1.0 ± 0.04	3.5 ± 0.4	0.5 ± 0.04	0.3 ± 0.03	0.5 ± 0.05
Apr.	374.4 ± 0.2	376.6 ± 0.2	1.1 ± 0.05	3.1 ± 0.2	0.4 ± 0.08	0.6 ± 0.05	0.6 ± 0.05
May	373.9 ± 0.2	372.5 ± 0.8	1.6 ± 0.07	7.2 ± 0.4	−0.4 ± 0.22	1.4 ± 0.11	−0.4 ± 0.05
June	370.8 ± 0.1	365.6 ± 0.7	1.9 ± 0.09	8.7 ± 0.4	−1.8 ± 0.24	2.0 ± 0.19	−1.6 ± 0.14
July	366.8 ± 0.3	357.6 ± 0.7	2.0 ± 0.07	10.8 ± 0.4	−1.8 ± 0.24	2.4 ± 0.19	−2.5 ± 0.18
Aug.	363.9 ± 0.2	358.3 ± 0.9	1.8 ± 0.08	10.8 ± 0.4	−1.1 ± 0.21	2.0 ± 0.16	−1.3 ± 0.10
Sep.	363.7 ± 0.3	366.1 ± 0.7	1.7 ± 0.08	7.4 ± 0.4	0.2 ± 0.19	1.5 ± 0.14	0.6 ± 0.07
Oct.	366.9 ± 0.1	371.9 ± 0.8	1.1 ± 0.06	5.1 ± 0.4	0.6 ± 0.08	0.6 ± 0.07	1.1 ± 0.08
Nov.	370.7 ± 0.2	375.9 ± 0.4	1.0 ± 0.05	3.2 ± 0.2	0.6 ± 0.07	0.2 ± 0.04	0.5 ± 0.09
Dec.	372.8 ± 0.2	375.6 ± 0.4	0.7 ± 0.02	1.5 ± 0.1	0.4 ± 0.05	0.1 ± 0.02	0.4 ± 0.05

[a] C_t values are from the marine boundary layer at 44.4°N- GLOBALVIEW data set. C_m and q_m values are from continuous measurements of CO_2 from the WLEF tower (396 m). The q_t values are from RUC data.
[b] Propagated error was determined from the monthly standard deviation for all variables in equations (1) and (3).

COBRA campaign; *Gerbig et al.* [2003]). The large dashed line is the CO_2 mixing ratio for the marine boundary layer (MBL) at 44.4°N or ''background CO_2'' which was derived from monthly measurements by NOAA-CMDL (GLOBALVIEW-CO_2, 2003; see ftp.cmdl.noaa.gov,Path:ccg/co2/GLOBALVIEW). The short dashed line represents monthly averages of CO_2 sampled weekly by NOAA-CMDL at 3475 m atop Niwot Ridge, CO, USA (40.05°N). We use the MBL values for C_t throughout our analysis because 44.4°N is nearly the same latitude as the WLEF tower. The limited available data suggest that CO_2 measured in the MBL is reasonably representative (on monthly timescales) of CO_2 in the free troposphere above the WLEF tower. *Yi et al.* [2004] and data collected from the COBRA program (in the years 2000 and 2003, http://www-as.harvard.edu/chemistry/cobra/) show little vertical stratification in CO_2 above the ABL for several locations over North America. Further, on a seasonal average there was only a 0.3 ppmv gradient between observations of CO_2 made in the North Pacific to those made in the North Atlantic [*Fan et al.*, 1998]. We do not suggest here that actual free-tropospheric CO_2 is invariable. Rather, we suggest that over monthly timescales there is a larger difference in CO_2 mixing ratio from the ABL to the free troposphere in one latitude than there is within the free troposphere across latitudes, which is expected as strong zonal winds mix the free troposphere in midlatitudes [*Peixoto and Oort*, 1992]. Figure 1b offers nominal support for this assumption, as there is little difference between CO_2 in the MBL, Niwot Ridge, and the direct aircraft measurements of free-tropospheric CO_2. We offer further support for this assumption below, showing that calculations of net CO_2 flux (F_{NEE}) are reasonably similar when using C_t values from either the MBL at 44.4°N or Niwot Ridge at 40.05°N.

[17] While CO_2 is quite well mixed in the free troposphere, water vapor (q) is not because of the decrease of saturation vapor pressure with temperature. However, in undisturbed conditions without precipitation, the mixing processes through the ABL conserve water as well as CO_2. Hence we define differences in q between the ABL (q_m) and an average of 3000–3700 m (ASL- ground level is approximately 500 m) which we take as representative of free-tropospheric air entering the ABL (q_t). Direct measurements of average q_t in the month of August nearly matched q_t derived from Rapid Update Cycle weather forecast analysis. Based solely on this agreement between RUC outputs and observed data for one month, we assumed that the RUC data provided an acceptable measure of monthly q_t for the year of 2000. The determination of ρW_{FD} by (4) is, however, relatively insensitive to q_t as the monthly average q_t was always 1/3 to 1/10 of q_m (see Table 2 and sensitivity analysis below).

[18] The idealized equilibrium boundary layer model considers the ABL solely under the subsiding branch of the synoptic cycle and Figure 2 shows how the key variables in the equilibrium equations (2) and (4) change as more disturbed days with greater rainfall, are removed from the monthly averages (see section 2.5). Not surprisingly, there was a general trend for increasing mean F_q as rainy days were removed from the monthly averages (Figure 2a), which is indicative of less evapotranspiration during rainy periods that are typically cloudier. The precipitation filter has little impact on $\Delta q = q_t - q_m$ and $\Delta C = C_t - C_m$ on the monthly timescale (Figures 2b and 2c). As storms move through, C_m and q_m can change dramatically from day to day and even from minute to minute as the strong vertical mixing associated with storms tends to replace ABL air with free-tropospheric air [*Hurwitz et al.*, 2004]. Yet it is apparent from Figures 2b and 2c that a coherent structure of the vertical difference of ABL scalars develops on a monthly basis. Such consistent monthly structure in Δq and ΔC is particularly interesting considering that from May to September the ''ppt < 1 mm'' mean values had nearly 30% fewer days in the monthly averages than the ''all days'' mean values (Table 1).

3.2. Estimates of ρW on Monthly Timescales

[19] ρW calculated by the flux difference method (equation (4); ρW_{FD}) showed substantial variation throughout the year (Figure 3), but generally followed expected annual patterns for mean vertical velocity [*Stull*, 1988]. ρW_{FD} was the largest from April through September when increased solar input would be expected to amplify vertical transports by convection. There was little effect of removing rainy days from the calculations of ρW_{FD} except in the months June, July and September. These months coincide with large differences in F_q across the different levels of the precipitation filter, while there were virtually no differences in Δq over the same time period (Figure 2a). Hence it

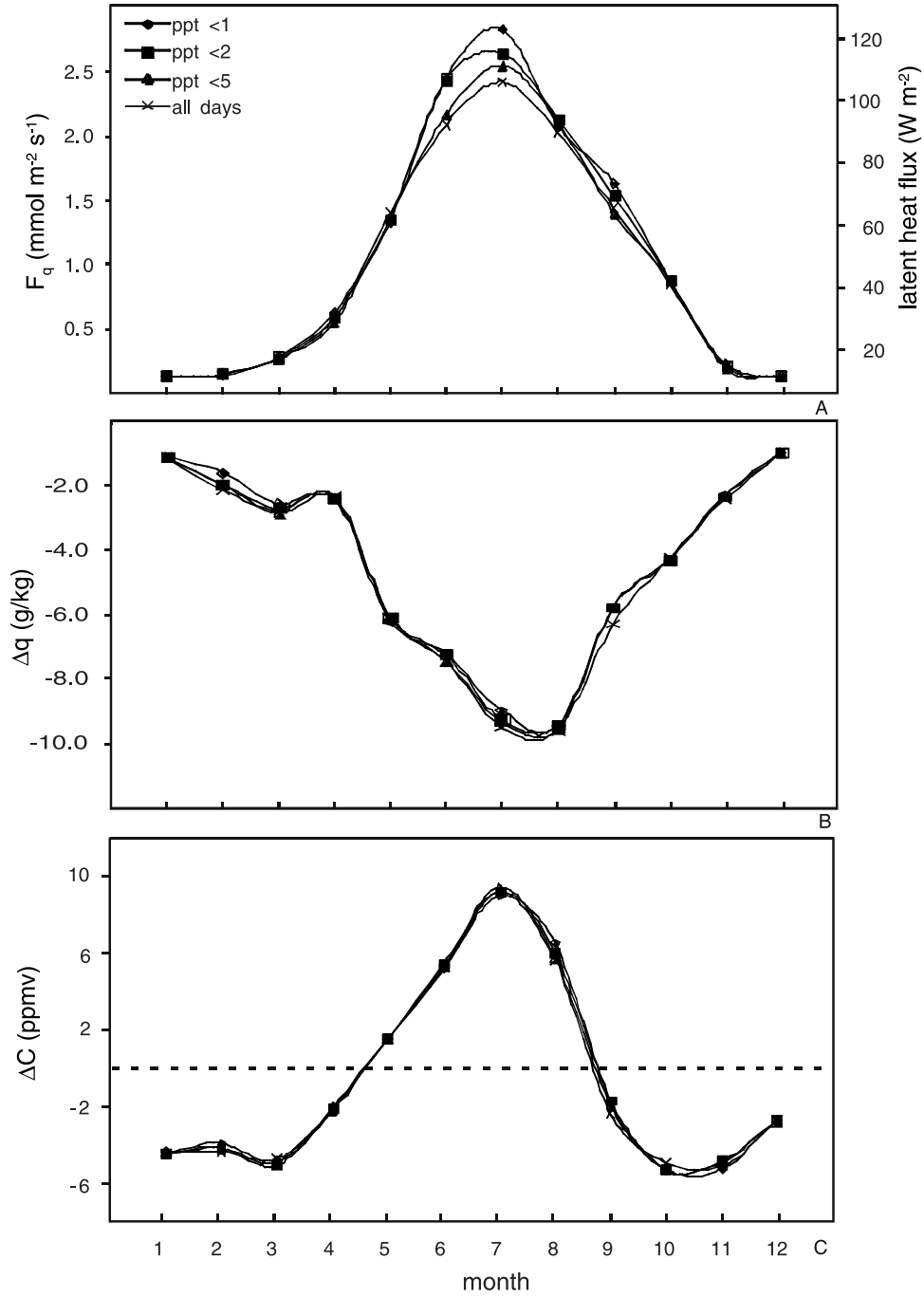

Figure 2. Monthly means for all days in a month and the precipitation filters applied to (a) water vapor flux (F_q), (b) the ABL to free troposphere water vapor difference (Δq; $q_t - q_m$), and (c) the ABL to free troposphere CO_2 difference (ΔC; $C_t - C_m$). See color version of this figure in the HTML.

appears that the larger "fair weather" fluxes of F_q are the driving force behind the increasing values of ρW_{FD} in June, July and September as rainy periods are removed from the monthly averages.

[20] The comparison of ρW_{FD} estimates with ρW estimates from reanalysis-2 data (ρW_Ω) supports our general hypothesis that the flux of dry air into the ABL nearly balances surface evapotranspiration, and that large-scale synoptic subsidence plays a dominant role in maintaining ABL equilibrium. The monthly averaged ρW_Ω values from reanalysis-2 data for days when ppt < 1 mm and for all days in a month are presented in Figure 4. The "daily average" ρW_Ω from the reanalysis is noisy because it is an average of instantaneous values which are archived only four times per day. The vertical velocity in a forecast model contains higher frequency gravity wave "noise," which is very poorly sampled at this six-hour frequency, so we do not have a true 24 hour mean. The monthly mean shown fluctuates around zero, and ρW_Ω becomes more negative as rainy days are excluded. This is an expected result as

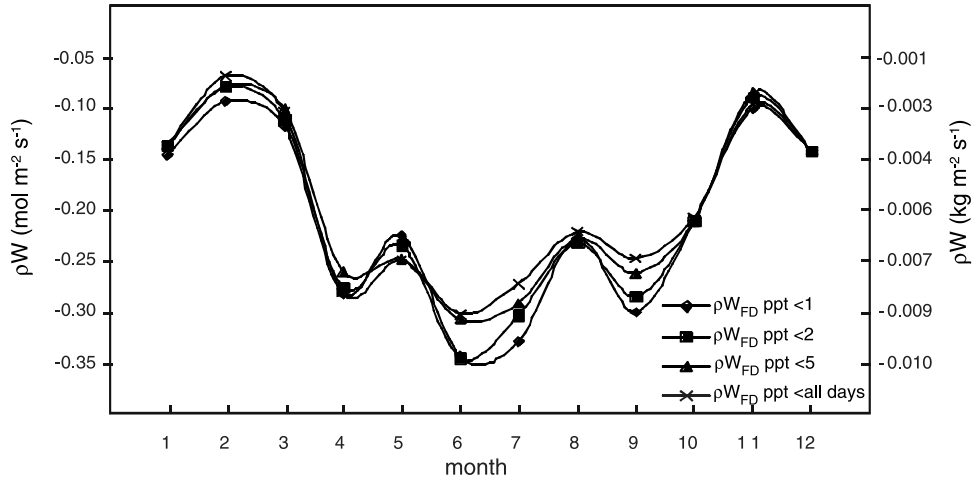

Figure 3. Estimates of monthly mean vertical velocity determined by the flux difference method (ρW_{FD}; equation (3)) for all days in a month and with precipitation filters ppt < 1, 2, and 5 mm applied. F_q was derived from eddy covariance measurements, q_m measured from the WLEF tower and q_t from RUC reanalysis data. See color version of this figure in the HTML.

precipitation tends to occur during periods of mean ascent. The monthly ρW_Ω estimates at ppt < 1 mm showed a fairly similar annual pattern as ρW_{FD} estimates, peaking in summer, but with a reduced magnitude. Our derived value of ρW_{FD} is larger than the mean subsidence ρW_Ω for ppt < 1 mm by about 0.05 mol m^{-2} s^{-1}, 0.002 kg $m^{-1}s^{-1}$ or about 20 hPa d^{-1}. This probably reflects the fact that the ABL is not in exact equilibrium, but is recovering and growing at this slow rate (and therefore entraining more tropospheric air) for periods of several days between each rainy disturbance, which typically occupy only a rather small temporal fraction. However, to make such conclusions, we need better estimates of ρW_Ω than those currently available from reanalysis, particularly to resolve shorter time periods. Figure 4 shows that by removing days when ascent dominates the monthly averaged estimates of ρW_{FD} and ρW_Ω start to converge which suggest that the flux of dry air into the ABL roughly balances surface water vapor flux and that large-scale subsidence controls ABL equilibrium.

3.3. Net CO_2 Exchange

[21] Monthly estimates of F_{NEE} were determined by (2) with the monthly mean CO_2 differences and the corresponding values of ρW_{FD} (Figure 5a). As with the comparisons of ρW_{FD}, the estimates of F_{NEE} were nearly indistinguishable across the precipitation filters with the exception of June and July. The differences in CO_2 did not change by including or removing days when precipitation occurred (Figure 2c); so ρW_{FD} was clearly the driver of variability for the summer estimates of F_{NEE}. However, the distinct difference in ρW_{FD} that was observed in September was not manifested in distinct values of F_{NEE} due to the small overall ABL-to-free tropospheric difference in CO_2. The monthly averages of NEE estimated by EC measure-

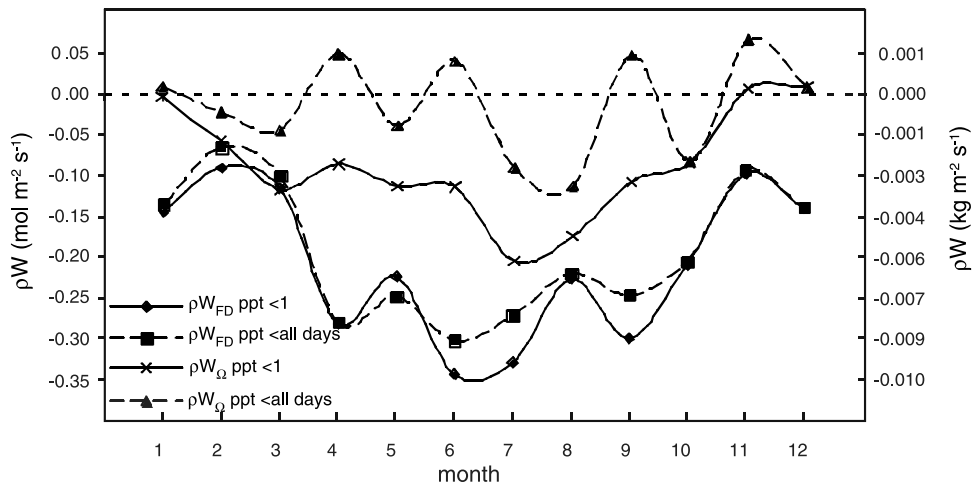

Figure 4. Estimates of mean vertical velocity determined by the flux difference method (ρW_{FD}) and from NCEP/NCAR reanalysis-2 model data. Monthly means are presented for all days in a month and with precipitation filters ppt < 1 mm. See color version of this figure in the HTML.

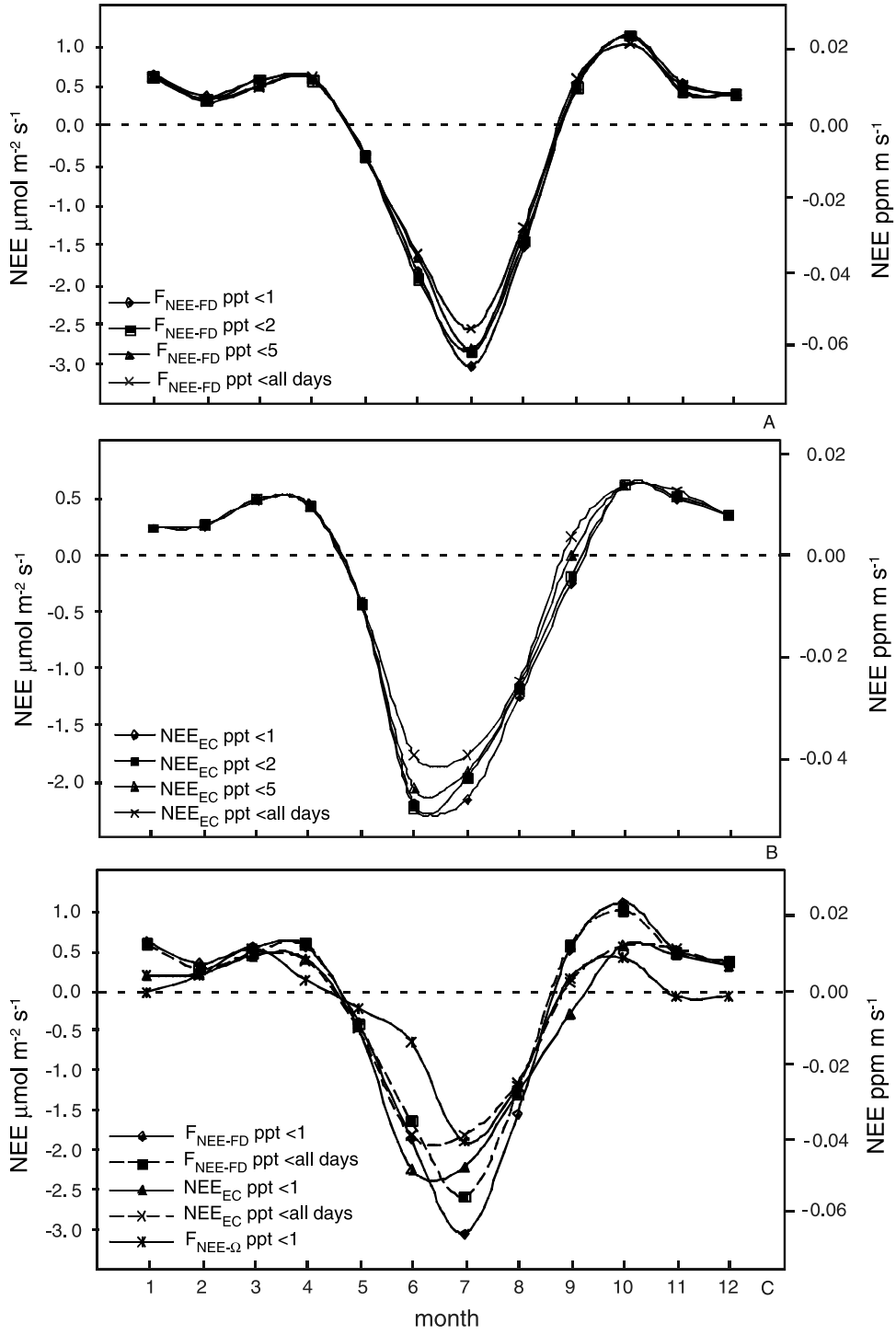

Figure 5. Net ecosystem exchange for CO_2 (NEE) (a) as determined by equation (1) ($F_{NEE\text{-}FD}$) and using the ρW estimates from Figure 3 and (b) from eddy covariance estimates for all days in a month and with precipitation filters ppt < 1, 2, and 5 mm applied. (c) F_{NEE} determined by the reanalysis-2 data derived ρW_Ω ($F_{NEE\text{-}\Omega}$) for ppt < 1 is presented with NEE_{EC} and $F_{NEE\text{-}FD}$ for direct comparison of estimates. See color version of this figure in the HTML.

ments at 122 m from the WLEF tower (NEE_{EC}) are shown in Figure 5b. As more disturbed days were removed from the analysis of NEE_{EC}, the monthly average NEE increased, particularly in summer. This trend was similar to the observed trend of increasing F_q with decreasing rainy days in the monthly averages and is possibly a result of decreased carbon uptake under overcast skies during disturbed periods. The monthly averages of NEE_{EC} and F_{NEE} for ppt < 1 mm and "all days" are presented together in Figure 5c for direct comparison. Also in Figure 5c is the mean monthly F_{NEE} estimated using the smaller ρW_Ω under the ppt < 1 mm filter. The most obvious feature in Figure 5c is the remark-

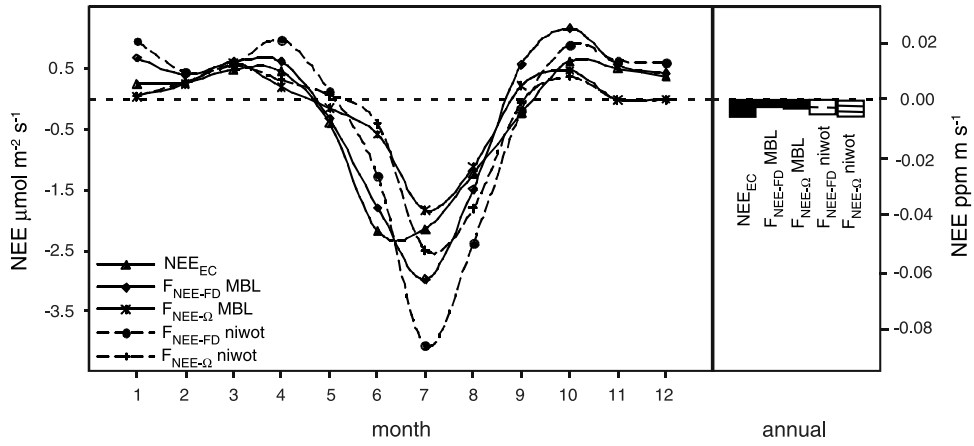

Figure 6. Net ecosystem exchange for CO_2 calculated using either the marine boundary layer (MBL) or Niwot Ridge (niwot) for free-tropospheric CO_2. All calculations were made using the ppt < 1 filter. See color version of this figure in the HTML.

able similarity of the independent estimates of NEE. The three estimates of NEE showed similar sink-to-source phase shifts and there was good agreement between the estimates on a monthly basis. We do not explicitly include fossil fuel emissions in our regional analysis, but the surface footprint that affects C_m includes a larger fossil fuel flux component than the eddy correlation footprint. It is possible that the differences between F_{NEE} (ρW_{FD}) and NEE_{EC} reflect different fossil fuel emissions within the different footprints, but further study is required to quantify these flux differences.

[22] Flux calculations using C_t from Niwot Ridge and MBL were compared to test the impact the different free-tropospheric proxies have on F_{NEE} (Figure 6). For each month, the F_{NEE} estimates were fairly close using either MBL or Niwot ridge for C_t with the exception of the F_{NEE} (ρW_{FD}) estimates in July when mean CO_2 for MBL and Niwot Ridge were not well matched. Further tests of how well MBL or mountain top measurements represent actual free-tropospheric CO_2 need to be conducted directly using airplane measurements and are part of the North American Carbon Plan. Also in Figure 6 are the annual averages of CO_2 flux which showed little difference between all estimates of net surface CO_2 flux. The overall agreement between the various methods for calculating F_{NEE} and NEE_{EC} (Figures 5 and 6) shows that, on longer timescales, the vertical flux of CO_2 from the free troposphere is in near balance with the net CO_2 flux at the surface.

3.4. Mixing and Matching Footprints

[23] The footprint of 122 m EC measurements from the WLEF tower includes hardwood deciduous, aspen and pine forests, bog sites and open water. These land cover types repeat in a self-similar fashion in areas extending about 150 km east, west and south of the tower, and about 70 km north of the tower where land gives way to Lake Superior. To calculate ρW_{FD}, F_q was measured locally by EC and had a footprint on the order of 1 km^2. Considering the mixing height of the ABL and the movement of the ABL over the land surface, the footprint affecting the mixing ratio of C_m and q_m was undoubtedly much larger. *Gloor et al.* [2001] estimated that the footprint controlling C_2Cl_4 mixing ratio (and by inference, CO_2) at the WLEF tower was on the order of 10^6 km^2, and other published estimates of surface area affecting scalar mixing ratios in the ABL range from 10^3 to 10^5 km^2 [*Raupach et al.*, 1992; *Styles et al.*, 2002]. We assumed that EC estimates of F_q made from the tower were fairly representative of the region as a whole. However, it would obviously be preferable to obtain estimates of F_q over a spatial scale that is representative of C_m and q_m.

[24] Figure 7 compares the EC local value of F_q with monthly averages from the NCEP/NCAR reanalysis-2 (surface footprint of about 3×10^4 km^2). The two estimates of F_q are closely matched for July through October. However, for the rest of the year F_q from the reanalysis-2 data appears to be unrealistically large. For example, in March and April when average temperatures are below freezing and the deciduous trees have yet to flush leaves the Reanalysis F_q was only about 25% less than August. Surface flux products from different models and reanalyses show considerable variability in the surface evaporation coming from different land-surface models and analysis methods [*Roads and Betts*, 2000; *Roads et al.*, 2003; *Berbery et al.*, 2003; *Betts et al.*, 2003], so it is clear we do not yet have accurate regional estimates of surface fluxes from models, although improvements are continually being made.

[25] This success of the flux difference method suggests that vertical exchange between the ABL and the free troposphere dominates the continental ABL CO_2 budget over seasonal timescales. This vertical exchange explains the seasonal phase lag between ABL CO_2 mixing ratios and NEE of CO_2 noted in the WLEF data [*Davis et al.*, 2003] and explored for multiple sites by *Bakwin et al.* [2004]. Further, *Bakwin et al.* [2004] adopted a modification of our method using only the reanalysis-2 data and extended it with reasonable success to multiple sites, suggesting that these results are not unique to the northern Wisconsin region.

3.5. Sensitivity Analysis

[26] The importance of each measured variable in calculating F_{NEE} using the flux difference method (ρW_{FD}) was assessed individually by performing a sensitivity analysis over "all days" using the standard error of the mean for

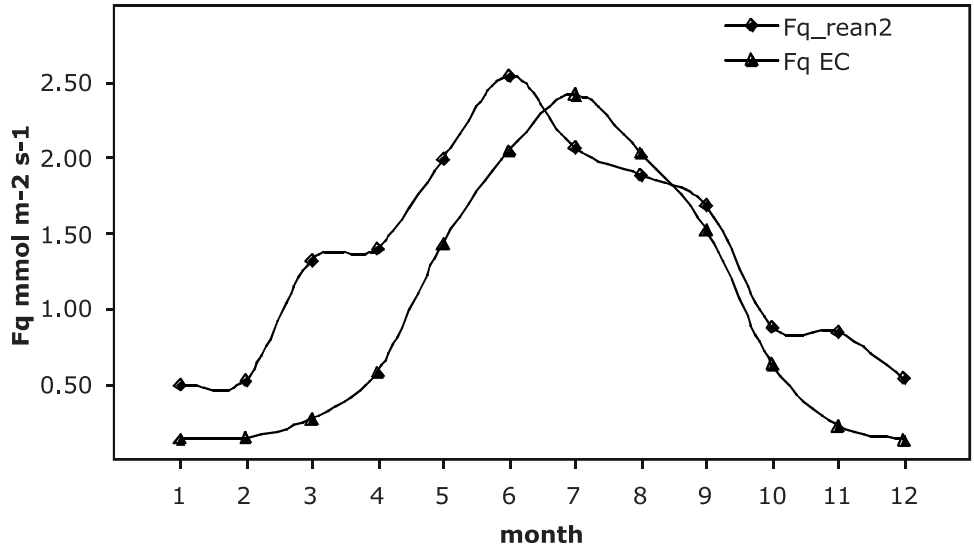

Figure 7. Monthly averages of molar water vapor flux (F_q) measured by eddy covariance at 122 m (blue triangles) on the WLEF tower and from NCEP/NCAR reanalysis-2 data (red diamonds). See color version of this figure in the HTML.

each variable (listed in Table 2). The standard error for each month was calculated assuming that each 24 hour period was one independent sample for the monthly mean. The results of the sensitivity analysis are presented in Table 3. F_{NEE} was least sensitive to q_t, which is not surprising as free-tropospheric water vapor from 2500 to 3200 m was relatively constant and near 1.3 g kg^{-1} on an annual basis. Therefore a precise measurement of q_m is more important than q_t in calculating the water vapor difference between the ABL and the free troposphere. The most important variable in matching F_{NEE} to eddy covariance measurements of NEE was C_m, followed by F_q, C_t and q_m. Hence accurate measurements of F_q, q_m and ($C_m - C_t$) are crucial to flux calculation by the ABL-flux method. Note that the standard error of the mean for C_m and C_t was on the order of measurement precision (0.1 ppmv).

[27] The propagated errors associated with F_{NEE} (Table 2) and the sensitivity analysis (Table 3) are obviously only a partial consideration of the error involved in calculating the net flux. Our assumptions that F_q measured by EC represents regional F_q, and that C_t can be appropriately represented by the use of proxies rather than direct measurements represent potentially large sources of error for estimates of F_{NEE} by the flux difference approach; error sources which are not currently quantifiable. We used the reanalysis-2 data in an attempt to assuage the concern about asynchrony in F_q estimates, unfortunately the surface flux from the reanalysis-2 data appears to be unrealistically large for a part of the year. However, there are more robust land-coverage-based methods for estimating the largely unidirectional flux of water vapor for future tests of the flux difference method [*Anderson et al.*, 1997, 2000; *Mackay et al.*, 2002]. During storms water vapor is not conserved; however, both the surface flux and the water vapor difference between the ABL and free troposphere are small during these periods. Although water vapor is used here as the reference gas to obtain CO_2 transport, other gases such as radon, which is produced in the soil, might be another option. The representativeness of MBL proxies for C_t can be confirmed by regular aircraft soundings over the continent which will be an integral component of the North American Carbon Plan [*Wofsy and Harris*, 2002]. Furthermore, caution is needed when comparing these results to published eddy covariance flux estimates [e.g., *Davis et al.*, 2003] since our calculations have not taken into account period of missing data (14%) or times with low turbulence. The addition of data from more terrestrial towers and regular airplane flights, in concert with atmospheric transport models of free-tropospheric CO_2, would no doubt help constrain regional estimates of F_{NEE}.

4. Conclusions

[28] By approaching average CO_2 and water vapor mixing ratios in the ABL as a quasi-equilibrium problem, and making some simple assumptions about free-tropospheric

Table 3. Sensitivity Analysis for $F_{NEE\text{-}FD}$[a]

	Percent Change From Estimated F_{NEE} All Days				
Month	F_q + sem	C_t + sem	C_m + sem	q_t + sem	q_m + sem
Jan.	25	4	12	2	11
Feb.	20	3	8	1	12
Mar.	10	3	13	1	11
Apr.	9	9	10	2	7
May	8	14	56	1	6
June	9	3	13	1	5
July	8	4	8	1	4
Aug.	8	4	16	0	0
Sep.	9	13	29	1	6
Oct.	11	2	15	1	8
Nov.	19	3	7	2	7
Dec.	15	6	13	2	7
Mean (year)	13	6	17	1	7
Mean (May–Sep.)	8	7	24	1	4

[a]One standard error was added to each input individually while holding the other inputs constant to calculate the percent change in F_{NEE} relative to the $F_{NEE\text{-}FD}$ values presented in Figure 5.

boundary conditions, we were able to estimate net CO_2 surface exchange for an entire year from surface measurements of evaporation. These ABL-scale net CO_2 estimates were comparable to measurements made by eddy covariance techniques over this same time period. This lends observational support to the underlying hypothesis outlined in the introduction: that on timescales longer than a day and in subsiding regimes the ABL structure of water vapor and CO_2 represents a near-balance between the surface fluxes and the mixing-down of air from the free troposphere, and the fluxes can be represented by a mass exchange with the free troposphere and the difference of CO_2 and water vapor between the ABL and the free troposphere. It is obvious, however, that the full potential of this method requires more complete and systematic data, especially for CO_2 and water vapor in the free troposphere. New global and regional reanalyzes may also provide better regional estimates of surface evaporation for comparison with eddy correlation data. Recognizing the large surface area which affects scalars in the ABL over synoptic timescales, the flux difference approach presented here could provide useful regional- to continental-scale observational constraints on the net surface CO_2 flux for comparison with model estimates.

Appendix A

[29] The 396 m measurement height of C_m is generally above the nocturnal inversion and is nearly always below the capping inversion separating the ABL from the overlying free troposphere. Continuous measurements from this height, therefore, reflect changes in the daytime convective boundary layer and the nighttime residual layer through time $\left(\frac{\partial C_m}{\partial t}\right)$ [*Yi et al.*, 2001]. *Cotton et al.* [1995] showed that is a on a global average ABL air is replaced by free-tropospheric air every four days, so on these longer timescales, we assume that horizontal advection becomes less important than vertical advection and mixing across the substantial jump in CO_2 concentration associated with the capping inversion of the ABL. We therefore use a simplified budget equation for the ABL with depth h and mean CO_2 concentration C_m in which we neglect horizontal advection. As the ABL deepens in a subsiding mean flow $\overline{W}$ it entrains air from the free troposphere above with properties C_t, and we can write the budget equation for the ABL as [*Betts*, 1992]

$$\frac{\partial}{\partial t}(\rho h C_m) = F_{NEE} + \rho\left(\frac{\partial h}{\partial t}\right)C_t - \rho\overline{W}(C_t - C_m), \qquad (A1)$$

where F_{NEE} is the net surface CO_2 flux ($F_{photosynthesis}$ + $F_{respiration}$) in flux density units. Rearranging and ignoring the time variation of ρ gives

$$\rho h\frac{\partial C_m}{\partial t} = F_{NEE} - \rho W(C_t - C_m), \qquad (A2)$$

where $W = \left(\frac{\partial h}{\partial t}\right) - \overline{W}$ is the entrainment rate of the ABL, or the rate at which the ABL mixes in air from the free troposphere ($\overline{W}$ is typically negative corresponding to mean subsidence). In strict equilibrium, $\frac{\partial C_m}{\partial t} = \frac{\partial h}{\partial t} = 0$ and we get

$$F_{NEE} = \rho W(C_t - C_m) = \rho\overline{W}(C_t - C_m). \qquad (A3)$$

A similar equation to equation (A2) can be written for water vapor

$$\rho h\frac{\partial q_m}{\partial t} = F_q - \rho W(q_t - q_m). \qquad (A4)$$

Following *Raupach et al.* [1992], we can assume a similar ABL entrainment rate for C and q. Dividing equation (A2) by equation (A4), and neglecting the time rate of change terms $\left(\frac{\partial C_m}{\partial t}, \frac{\partial q_m}{\partial t}\right)$ which become small compared to the flux terms over longer averaging periods (see Table A1) gives

$$\overline{F_{NEE}} = \frac{(\overline{C_t} - \overline{C_m})}{(\overline{q_t} - \overline{q_m})} \bullet \overline{F_q}. \qquad (A5)$$

Table A1. Rate of Change and Flux Terms for CO_2 and H_2O as the Averaging Period Increases[a]

	F_{NEE}, μmol m^{-2} s^{-1}	$\frac{\partial C_m}{\partial t}h$, μmol m^{-2} s^{-1}	F_q, μmol m^{-2} s^{-1}	$\frac{\partial q_m}{\partial t}h$, μmol m^{-2} s^{-1}
Sequence (2–7 Aug.)	−1.42	0.21	2.31	0.03
Aug.	−1.79	0.02	2.03	0.01
June–Aug.	−1.80	−0.06	2.18	0.02

[a]Assuming mean h of 1500 m.

[30] **Acknowledgments.** We are grateful to D. Fitzjarrald, R. Strand, P. Tans, R. Teclaw, S. Wofsy for theoretical and technical help with this study and the State of Wisconsin Educational Communications Board for access to the WLEF tower. This work was supported by grants from the National Oceanic and Atmospheric Administration (NAO6-GP-409), the National Science Foundation (TECO; DEB-9814194) and the Department of Energy (NIGEC; DEFC03-90ER61010 and DOE/DE-FG02-97ER62457). AKB was supported by NSF (ATM-9988618) and NASA (NAG5-11578).

References

Anderson, M. C., J. M. Norman, G. R. Diak, W. P. Kustas, and J. R. Mecikalski (1997), A two-source time-integrated model for estimating surface fluxes using thermal infrared remote sensing, *Remote Sens. Environ.*, *60*, 195–216.

Anderson, M. D., J. M. Norman, T. P. Meyers, and G. R. Diak (2000), An analytical model for estimating canopy transpiration and carbon assimilation fluxes based on canopy light-use efficiency, *Agric. For. Meteorol.*, *101*, 265–289.

Bakwin, P. S., P. P. Tans, D. F. Hurst, and C. Zhao (1998), Measurements of carbon dioxide on very tall towers: Results of the NOAA/CMDL program, *Tellus*, *Ser. B*, *50*, 401–415.

Bakwin, P. S., K. J. Davis, C. Yi, S. C. Wofsy, J. W. Munger, L. Haszpra, and Z. Barcza (2004), Regional carbon dioxide fluxes from mixing ratio data, *Tellus*, *Ser. B*, *56*, 301–311.

Baldocchi, D., et al. (2001), FLUXNET: A new tool to study the temporal and spatial variability of ecosystem-scale carbon dioxide, water vapor and energy flux densities, *Bull. Am. Meteorol. Soc.*, *82*, 2415–2434.

Berbery, E. H., Y. Luo, K. E. Mitchell, and A. K. Betts (2003), Eta model estimated land surface processes and the hydrologic cycle of the Mississippi basin, *J. Geophys. Res.*, *108*(D22), 8852, doi:10.1029/2002JD003192.

Betts, A. K. (1992), FIFE atmospheric boundary layer budget methods, *J. Geophys. Res.*, *97*, 18,523–18,532.

Betts, A. K. (2000), Idealized model for equilibrium boundary layer over land, *J. Hydrometeorol.*, *1*, 507–523.

Betts, A. K. (2004), Understanding hydrometeorology using global models: American Meteorological Society Robert Horton Lecture, E., January 14, 2004, Seattle, *Bull. Am. Meteorol. Soc.*, in press.

Betts, A. K., and J. H. Ball (1998), FIFE surface climate and site-average dataset 1987–89, *J. Atmos. Sci.*, *55*, 1091–1108.

Betts, A. K., and W. L. Ridgway (1989), Climatic equilibrium of the atmospheric convective boundary layer over a tropical ocean, *J. Atmos. Sci.*, *46*, 2621–2641.

Betts, A. K., J. H. Ball, M. Bosilovich, P. Viterbo, Y. Zhang, and W. B. Rossow (2003), Intercomparison of water and energy budgets for five Mississippi subbasins between ECMWF reanalysis (ERA-40) and NASA Data Assimilation Office fvGCM for 1990–1999, *J. Geophys. Res.*, *108*(D16), 8618, doi:10.1029/2002JD003127.

Betts, A. K., B. R. Helliker, and J. A. Berry (2004), Coupling between CO2, water vapor, temperature and radon and their fluxes in an idealized equilibrium boundary layer over land, *J. Geophys. Res.*, *109*, D18103, doi:10.1029/2003JD004420.

Ciais, P., P. P. Tans, M. Trolier, J. W. C. White, and R. J. Francey (1995), A large Northern Hemisphere terrestrial CO2 sink indicated by the 13C/12C ratio of atmospheric CO2, *Science*, *269*, 1098–1102.

Ciais, P., et al. (1997), A three-dimensional synthesis study of $\delta^{18}O$ in atmospheric CO_2: 2. Simulations with the TM2 transport model, *J. Geophys. Res.*, *102*, 5873–5883.

Conway, T. J., P. P. Tans, L. S. Waterman, K. W. Thoning, D. R. Kitzis, K. A. Masarie, and N. Zhang (1994), Evidence for interannual variability of the carbon cycle from the National Oceanic and Atmospheric Administration/Climate Monitoring and Diagnostics Laboratory Global Air Sampling Network, *J. Geophys. Res.*, *99*(D11), 22,831–22,855.

Cotton, W. R., G. D. Alexander, R. Hertenstein, R. L. Walko, R. L. McAnelly, and M. Nicholls (1995), Cloud venting—A review and some new global annual estimates, *Earth Sci. Rev.*, *39*, 169–206.

Davis, K. J., P. S. Bakwin, B. W. Berger, C. Yi, C. Zhao, R. M. Teclaw, and J. G. Isebrands (2003), Long-term carbon dioxide fluxes from a very tall tower in a northern forest: Annual cycle of CO2 exchange, *Global Change Biol.*, *9*, 1278–1293.

De Bruin, H. A. R. (1983), A model for the Priestley-Taylor parameter, α, *J. Clim. Appl. Meteorol.*, *22*, 572–578.

Denmead, O. T., M. R. Raupach, F. X. Dunin, H. A. Cleugh, and R. Leuning (1996), Boundary layer budgets for regional estimates of scalar fluxes, *Global Change Biol.*, *2*, 255–264.

Denning, A. S., I. Y. Fung, and D. Randall (1995), Latitudinal gradient of atmospheric CO2 due to seasonal exchange with land biota, *Nature*, *376*, 240–243.

Fan, S., M. Gloor, J. Mahlman, S. Pacala, J. Sarmiento, T. Takahashi, and P. Tans (1998), A large terrestrial carbon sink in North America implied by atmospheric and oceanic carbon dioxide data and models, *Science*, *282*, 442–446.

Fitzjarrald, D. R. (2002), Boundary layer budgeting, in *Vegetation, Water, Humans and the Climate: A New Perspective on an Interactive System*, edited by P. Kabat et al., pp. 239–254, Springer-Verlag, New York.

Fung, I., et al. (1997), Carbon 13 exchanges between the atmosphere and biosphere, *Global Biogeochem. Cycles*, *11*, 507–533.

Gerbig, C., J. C. Lin, S. C. Wofsy, B. C. Daube, A. E. Andrews, B. B. Stephens, P. S. Bakwin, and A. Grainger (2003), Toward constraining regional-scale fluxes of CO2 with atmospheric observations over a continent: 1. Observed spatial variability from airborne platforms, *J. Geophys. Res.*, *108*(D24), 4756, doi:10.1029/2002JD003018.

Gloor, M., P. Bakwin, D. Hurst, L. Lock, R. Draxler, and P. Tans (2001), What is the concentration footprint of a tall tower?, *J. Geophys. Res.*, *106*(D16), 17,831–17,840.

Gurney, K. J., et al. (2002), Towards robust regional estimates of CO2 sources and sinks using atmospheric transport models, *Nature*, *415*, 626–630.

Helliker, B. R., J. Berry, P. Bakwin, K. Davis, A. S. Denning, J. Ehleringer, J. Miller, M. Butler, and D. Ricciuto (2002), Measurements of regional-scale isotopic discrimination and CO_2 flux for the north-central U.S., *Eos Trans. AGU*, *83*, Fall Meet. Suppl., Abstract B71C-10.

Hurwitz, M. D., D. M. Ricciuto, K. J. Davis, W. Wang, C. Yi, M. P. Butler, and P. S. Bakwin (2004), Advection of carbon dioxide in the presence of storm systems over a northern Wisconsin forest, *J. Atmos. Sci.*, *61*, 607–618.

Keeling, C. D., et al. (1989), A three-dimensional model of atmospheric CO2 transport based on observed winds: 1. Analysis of observational data, in *Aspects of Climate Variability in the Pacific and the Western Americas*, *Geophys. Monogr. Ser.*, vol. 55, edited by D. H. Peterson, pp. 277–303, AGU, Washington, D. C.

King, D. B., and R. C. Schnell (Eds.) (2002), Climate monitoring and diagnostics laboratory summary, *Rep. 26*, *2000–2001*, NOAA/CMDL, Boulder, Colo.

Kuck, L. R., et al. (2000), Measurements of landscape-scale fluxes of carbon dioxide in the Peruvian Amazon by vertical profiling through the atmospheric boundary layer, *J. Geophys. Res.*, *105*(D17), 2137–2146.

Levy, P. E., A. Grelle, A. Lindroth, M. Molder, P. G. Jarvis, B. Kruijt, and J. B. Moncrieff (1999), Regional-scale CO2 fluxes over central Sweden by a boundary layer budget method, *Agric. For. Meteorol.*, *99*, 169–180.

Lloyd, J., et al. (2001), Vertical profiles, boundary layer budgets, and regional flux estimates for CO_2 and its $^{13}C/^{12}C$ ratio and for water vapor above a forest/bog mosaic in central Siberia, *Global Biogeochem. Cycles*, *15*(2), 267–284.

Mackay, D. S., D. E. Ahl, B. E. Ewers, S. T. Gower, S. N. Burrows, S. Samanta, and K. J. Davis (2002), Effects of aggregated classifications of forest composition on estimates of evapotranspiration in a northern Wisconsin forest, *Global Change Biol.*, *8*(12), 1253–1265.

McNaughton, K. G., and T. W. Spriggs (1986), A mixed-layer model for regional evaporation, *Boundary Layer Meteorol.*, *34*, 243–262.

Pattey, E., I. B. Strachan, R. L. Desjardins, and J. Massheder (2002), Measuring nighttime CO_2 flux over terrestrial ecosystems using eddy covariance and nocturnal boundary layer methods, *Agric. For. Meteorol.*, *113*, 145–158.

Peixoto, J. P., and A. H. Oort (1992), *Physics of Climate*, Springer-Verlag, New York.

Raupach, M. R. (1995), Vegetation-atmosphere interaction and surface conductance at leaf, canopy and regional scales, *Agric. Forest Meteorol.*, *73*, 151–170.

Raupach, M. R. (2000), Equilibrium evaporation and the convective boundary layer, *Boundary Layer Meteorol.*, *96*, 107–141.

Raupach, M. R. (2001), Combination theory and equilibrium evaporation, *Q. J. R. Meteorol. Soc.*, *127*, 1149–1181.

Raupach, M. R., O. T. Denmead, and F. X. Dunin (1992), Challenges in linking atmospheric CO_2 concentrations to fluxes at local and regional scales, *Aust. J. Botany*, *40*, 697–716.

Roads, J., and A. K. Betts (2000), NCEP/NCAR and ECMWF reanalysis surface water and energy budgets for the GCIP region, *J. Hydrometeorol.*, *1*, 88–94.

Roads, J., et al. (2003), GCIP Water and Energy Budget Synthesis (WEBS), *J. Geophys. Res.*, *108*(D16), 8609, doi:10.1029/2002JD002583.

Stull, R. B. (1988), *An Introduction to Boundary Layer Meteorology*, 666 pp., Kluwer Acad., Norwell, Mass.

Styles, J. M., J. Lloyd, D. Zolotoukhine, K. A. Lawton, N. Tchebakova, R. J. Francey, A. Arneth, D. Salamakho, O. Kolle, and E.-D. Schulze (2002), Estimates of regional surface carbon dioxide exchange and carbon and oxygen isotope discrimination during photosynthesis from concentration profiles in the atmospheric boundary layer, *Tellus*, *Ser. B*, *54*, 768–783.

Tans, P. P., I. Y. Fung, and T. Takahashi (1990), Observational constraints on the global atmospheric CO2 budget, *Science*, *247*, 1431–1438.

Wofsy, S. C., and R. C. Harris (2002), The North American Carbon Program (NACP): Report of the NACP Committee of the U.S. Interagency Carbon Cycle Science Program, U.S. Global Change Res. Program, Washington, D. C.

Yi, C., K. J. Davis, and B. W. Berger (2001), Long-term observations of the dynamics of the continental planetary boundary layer, *J. Atmos. Sci.*, *58*, 1288–1299.

Yi, C., K. J. Davis, P. S. Bakwin, A. S. Denning, N. Zhang, A. Desai, J. C. Lin, and C. Gerbig (2004), Observed covariance between ecosystem carbon exchange and atmospheric boundary layer dynamics at a site in northern Wisconsin, *J. Geophys. Res.*, *109*, D08302, doi:10.1029/2003JD004164.

P. S. Bakwin and J. B. Miller, Climate Monitoring and Diagnostics Laboratory, National Oceanic and Atmospheric Administration, 325 Broadway R/CMDL1, Boulder, CO 80305, USA.

J. A. Berry and B. R. Helliker, Department of Global Ecology, Carnegie Institution of Washington, 260 Panama St., Stanford, CA 94305, USA. (helliker@catalase.stanford.edu)

A. K. Betts, Atmospheric Research, Pittsford, VT 05763, USA.

M. P. Butler, K. J. Davis, and D. M. Ricciuto, Department of Meteorology, Pennsylvania State University, 512 Walker Building, University Park, PA 16802, USA.

A. S. Denning, Department of Atmospheric Science, Colorado State University, Fort Collins, CO 80523, USA.

J. R. Ehleringer, Department of Biology, University of Utah, 257S. 1400E., Salt Lake City, UT 84112, USA.